Annu. Rev. Earth Planet. Sci. 2001. 29:295–330

RHEOLOGICAL PROPERTIES OF WATER ICE—APPLICATIONS TO SATELLITES OF THE OUTER PLANETS[1]

WB Durham[2] and LA Stern[3]
[2]*University of California, Lawrence Livermore National Laboratory, Livermore, California 94550; e-mail: durham@llnl.gov*
[3]*US Geological Survey, Menlo Park, California 94025; e-mail: lstern@usgs.gov*

Key Words high-pressure phases, grain-size-sensitive creep, deformation mechanisms, brittle-to-ductile transition, Europa

■ **Abstract** The icy moons of the outer solar system have not been quiescent bodies, in part because many have a substantial water component and have experienced significant internal heating. We can begin to understand the thermal evolution of the moons and the rate of viscous relaxation of surface topography because we now have good constraints on how ice (in several of its polymorphic forms) flows under deviatoric stress at planetary conditions. Details of laboratory-derived flow laws for pure, polycrystalline ice are reviewed in detail. One of the more important questions at hand is the role of ice grain size. Grain size may be a dynamic quantity within the icy moons, and it may (or may not) significantly affect rheology. One recent beneficiary of revelations about grain-size-sensitive flow is the calculation of the rheological structure of Europa's outer ice shell, which may be no thicker than 20 km.

INTRODUCTION

The rheology of water ice has a first-order influence on the evolution and appearance of over 15 moons belonging to Jupiter and to planets beyond, many of which have a mass fraction of water >0.5. Internal heating and (sometimes) tidal flexing drive planetary convection. If ice flows readily, the planet is efficiently cooled; if ice resists flow, in the extreme the planet will overheat, begin to melt internally, and differentiate catastrophically. Warm ice flowing in the subsurface exerts tractions on a cold icy crust and, if it can support tractions sufficient to overcome the strength of the crust, may cause the crust to fail. On an icy crust, impact craters and other landforms relax under gravitational forces at a rate controlled by the viscosity of ice.

[1]The US Government has the right to retain a nonexclusive, royalty-free license in and to any copyright covering this paper.

Ice in terrestrial settings is arguably the most studied of geological materials, and a great body of literature exists describing its rheological properties. The "Glen law" for the creep of polycrystalline ice, relating strain rate to the third power of shear stress, and which owes its origins to one of the first systematic laboratory studies (Glen 1952, 1955), is still the rule of thumb for glaciologists. There is little overlap between conditions on Earth and those on icy moons, so when interest arose in icy moons in anticipation of space age advances in planetary exploration, there was little to constrain early prognostications of planetary dynamics. That situation has changed somewhat over the past two decades as space probes explored the outer solar system and computational methods improved and inspired modest laboratory investigation of the rheology of water ice and other frozen volatiles at more extreme pressures and temperatures.

This paper reviews the current state of knowledge of ice rheology at conditions applicable to icy satellites: where temperatures are very low at the surface (on the order of 100 K) and rise to terrestrial levels only at depths where lithostatic pressures are very high, and where deformation rates are geologically slow and unattainable in the laboratory. It is not our purpose to review the application of ice rheology to the satellites, although extended applications are given by way of example to illustrate the importance of a deeper understanding of rheology. The reader seeking the latter is our intended audience.

ICE IN THE OUTER SOLAR SYSTEM

Composition and Internal Structure of the Icy Satellites

Cosmochemical arguments predict abundant low-density, low-melting-point (<300 K), nonsilicate crystalline condensates in the outer solar system (Kargel 1998a; Lewis 1971, 1972; Prinn & Fegley 1981). Water predominates because of its overwhelming abundance in the solar system, but numerous other volatile compounds of hydrogen, oxygen, carbon, and nitrogen exist, with compounds of lower melting temperatures condensing farther from the sun (Lewis 1971, 1972). In the protoplanetary nebulae, the probable low-temperature condensation sequence in the region of the giant planets is only weakly pressure dependent and begins with water ice ($T < 200$ K), then compounds of ammonia and water ($T < 120$ K), then compounds of methane and water ($T < 60$ K) (Lewis 1972, Prinn & Fegley 1981). The details of composition of a moon are influenced by its path in temperature and pressure during condensation, but the best evidence is that temperatures in the Jovian system remained warm enough that Callisto, Ganymede, and certainly Europa condensed water ice with very little ammonia. At Saturn and beyond, $NH_3 \cdot H_2O$ probably did precipitate. Cooler temperatures in the protoplanetary nebulae at Uranus and Neptune favored N_2 and CO over NH_3 and CH_4. Reflectance spectroscopy shows that surface volatiles on most of the low-density moons are dominated by H_2O (Clark et al 1986, Cruikshank et al

1998a). Triton is an important exception, with a surface that is mostly N_2, with minor amounts of CO_2, CO, and CH_4, and possibly H_2O (Cruikshank et al 1993, 1998b). The only other body whose surface is not dominated by water is Pluto, which shows N_2, CH_4, and CO (but not CO_2) in addition to H_2O (Cruikshank et al 1998b), but its moon Charon shows mostly H_2O, with some $NH_3 \cdot H_2O$ and NH_3 (Brown & Calvin 2000, Marcialis et al 1987).

Actions that have shaped the moons include exogenic processes such as meteoritic bombardment, tidal forces resulting from orbital eccentricities, and solar and cosmic radiation, as well as endogenic processes such as radiogenic heating and phase changes, and resultant volume changes. Larger satellites are likely to have differentiated to some extent, as indicated by small moments of inertia (Showman & Malhotra 1999), although even some smaller moons, such as Enceledus, receive enough tidal heating to cause internal melting. The evidence for a past or present internal water or brine ocean on Europa is strong (Pappalardo et al 1998b, Kivelson et al 2000), and a strongly conducting Callisto may be explicable in terms of a briny internal ocean (see Showman & Malhotra 1999). Surface expressions of planetary-scale tectonic activity exist on nearly every large icy moon from Jupiter to Neptune with a few provocative exceptions, such as Callisto. Voyager imagery confirms planetary-scale tectonic activity on upward of 20 of these moons. Landforms from craters to chasms show varying degrees of viscous relaxation. Resurfacing by liquids or low-viscosity solids is common throughout the outer solar system. Surface ages range from very old (Callisto) to very young (Europa).

The Role of Ice Rheology—Overview

The rheology of ice has a substantial influence on planetary thermal evolution and tectonics (Ellsworth & Schubert 1983; Kirk & Stevenson 1987; McKinnon 1998; Mueller & McKinnon 1988; Reynolds & Cassen 1979; Schubert et al 1981, 1986), on the origin and shape of landforms such as furrows and grooves and other types of faults (Golombek & Banerdt 1986, Herrick & Stevenson 1990, Pappalardo et al 1998a, Parmentier et al 1982), on the maximum height of topography (Dimitrov & Bar-Nun 1999, Johnson & McGetchin 1973), on the rate of viscous relaxation of craters and other landforms (Dombard & McKinnon 2000, Parmentier & Head 1981, Scott 1967, Thomas & Schubert 1988), on diapirism (Pappalardo et al 1998b, Schenk & Moore 1998), and on other geologic processes. Cryovolcanism as a solid-state rheological process is important on icy satellites (e.g. Schenk & Moore 1998) but usually involves volatiles in addition to water (in particular ammonia), so it is outside the scope of water-ice rheology. Impact cratering is another important planetary process not covered in this review. The immediate form of an impact crater (i.e. its shape and volume, and the appearance of a central pit or dome) is in fact strongly affected by the rheology of the target material (Fink et al 1984, Lange & Ahrens 1987, Schenk 1993), but the cratering process involves exceedingly high deformation rates and modes of deformation different from those discussed below.

LABORATORY MEASUREMENT CONSIDERATIONS

General Principles and Definitions

In the interest of avoiding ambiguities, we first develop a number of definitions and equations connected to rheology. A solid body placed under a state of stress responds instantaneously with an elastic strain and, in subsequent increments of time, will respond with increments of viscous strain. Strain rate is the ratio of the latter two quantities. The viscous strain includes a viscoelastic portion, which is (eventually) recovered when stress is removed, and an inelastic portion, which represents a yield or permanent change of shape. Because we are mainly interested in the large strains and low stresses of planetary environments, the elastic strains can be considered insignificant and are mostly ignored here.

We distinguish ductile strain and brittle strain as being the volume conservative and volume nonconservative components of inelastic strain. An alternative definition is that a ductile material retains its strength as it deforms (undergoes strain), whereas a brittle material tends to lose strength (Jaeger & Cook 1976). These two definitions are not in conflict because the physical mechanisms of brittle deformation always require the creation of fractures or microfractures (in the case of dense materials) or the collapse of porosity (in the case of porous materials), both of which are associated with volume change. Outside of the present section, where their use is unavoidable, we will not use such terms as plasticity and plastic strain because they have entirely different and well-entrenched definitions in different disciplines. The concept of brittle deformation was generally not appreciated by metallurgists who developed the first theories of plasticity to describe the behavior of materials that are mostly ductile (Hill 1950), so for instance it was implicit in the statement of a plastic yield criterion that volume was conserved. A material under load was considered elastic if it did not reach a certain yield criterion, and plastic if it did. It was found useful to adopt essentially the same yield criteria in rock mechanics even though volume was no longer necessarily conserved (Jaeger 1969), and many in the computational branches of geology now use the term plasticity to include any yield process, volume-conservative or otherwise. On the other hand, to most rock rheologists, the terms plastic and ductile are synonymous (Evans & Kohlstedt 1995).

Our main interest here is the ductile flow of ice. We postulate the existence of a functional relationship between the state of stress (σ_{ij}) in a solid and the ductile response of that solid, the strain rate ($\dot{\varepsilon}_{ij}$), at all relevant environmental conditions.

Stress and Strain Rate

The stress tensor σ_{ij} can be separated into hydrostatic and nonhydrostatic portions. Thus,

$$\sigma_{ij} = \sigma'_{ij} + \sigma_m \delta_{ij}, \delta_{ij} = 1 \text{ if } i = j \text{ and } \delta_{ij} = 0 \text{ if } i \neq j, \qquad (1)$$

where

$$\sigma_m = 1/3(\sigma_{11} + \sigma_{22} + \sigma_{33}). \tag{2}$$

The scalar σ_m is called the mean normal stress; the tensor $\sigma_m \delta_{ij}$ acts to change the volume but not the shape of a body that is uniform and isotropic. The tensor σ'_{ij} is called the deviatoric stress and acts to change shape but not volume.

There are several common scalar representations of σ_{ij} and σ'_{ij} that take advantage of higher symmetries of simpler problems and exercises, or which use terminology appropriate to the particular application. For instance, glaciologists commonly use the octahedral shear stress, i.e. the shear stress resolved on the so-called octahedral plane, which lies parallel to the face of an octahedron with vertices on the principal axes of the stress tensor:

$$\tau_{\text{oct}} = (2^{1/2}/3)\left(I_1^2 + 3I_2\right)^{1/2}, \tag{3}$$

where I_1 and I_2 are the first and second invariants of σ_{ij} (using the Einstein convention of summing over repeated indices):

$$I_1 = \sigma_{ii}$$

$$I_2 = \sigma_{12}^2 + \sigma_{23}^2 + \sigma_{31}^2 - (\sigma_{11}\sigma_{22} + \sigma_{22}\sigma_{33} + \sigma_{33}\sigma_{11}) \tag{4}$$

(Hill 1950). Mendelson (1968) offers a particularly readable derivation of these relationships. [For derivations with a rock mechanics perspective, see also Jaeger & Cook (1976).] Nye (1957) defined a slight variation on Equation 3, an effective shear stress τ_{eff} and effective strain rate $\dot{\varepsilon}_{\text{eff}}$ such that

$$2\tau_{\text{eff}}^2 = \sigma'_{ij}\sigma'_{ij} \tag{5a}$$

and

$$2\dot{\varepsilon}_{\text{eff}}^2 = \dot{\varepsilon}_{ij}\dot{\varepsilon}_{ij}. \tag{5b}$$

Equation 5a is the von Mises yield criterion, long respected in metallurgy as one of the more accurate predictors of the point where a polycrystalline material under a general state of stress will yield (Hill 1950). The octahedral and effective shear stresses are related as $3\tau_{\text{oct}}^2 = 2\tau_{\text{eff}}^2$.

In experimental rock mechanics (Jaeger & Cook 1976), hydrostatic confinement is often used to simulate earth conditions or to suppress brittle behavior. In the axisymmetric environment of the so-called triaxial deformation apparatus, it is convenient to view the yield criterion as the difference between the maximum stress, usually the stress applied by the operator to the end of a cylindrical sample, and the minimum stress, usually the fluid pressure (P) applied to the cylindrical

surface of the sample. Orienting σ_{11} with the maximum principal stress, $\sigma_{22} = \sigma_{33} = P$ and the yield criterion becomes

$$\sigma = \sigma_{11} - \sigma_{22} = \sigma_{11} - \sigma_{33} = \sigma_{11} - P, \tag{6}$$

where σ is called the maximum differential stress or simply differential stress. Equation 6 is the Tresca yield criterion (Hill 1950) and is the criterion of choice for the rheological data tabulated in this review. For axisymmetric flow, the yield criteria of Equations 3, 5a, and 6 differ by only a constant factor, so they are essentially equivalent. For plane strain, the same is true. For three-dimensional strain that is not axisymmetric, Equations 3 and 5a are demonstrably more accurate than Equation 6 (Hill 1950). Computational specialists in planetology have often adopted the more rigorous von Mises criterion (e.g. Ojakangas & Stevenson 1989, Thomas & Schubert 1987). Improvements on Equations 3 and 5a that use I_3, the third invariant of the stress tensor without the use of I_1, are theoretically even more accurate (Nye 1957).

Confusion often arises in the geological literature over differential vs deviatoric stress, and it is important to make the distinction correctly (Engelder 1994). In the axisymmetric case just discussed, the mean stress (Equation 2) is

$$\sigma_m = 1/3(\sigma + P + 2P) = P + (\sigma/3). \tag{7}$$

Thus, from Equations 1 and 6,

$$\sigma'_{ij} = \begin{pmatrix} \frac{2}{3}\sigma & 0 & 0 \\ 0 & -\frac{1}{3}\sigma & 0 \\ 0 & 0 & -\frac{1}{3}\sigma \end{pmatrix}. \tag{8}$$

It is imprecise and sometimes incorrect to speak of deviatoric stress in a scalar sense (e.g. a deviatoric stress of 1 MPa). As Engelder (1994) points out, it is not difficult to find examples of misuse in the literature. Usually what one means in such (mis)usage is one of the scalar quantities: Equations 3, 5a, or 6. The maximum differential deviatoric stress, for example, is identical to the maximum differential stress.

The Flow Law

A key principle in plasticity (i.e. ductility), stated as the Lévy-Mises equations (Hill 1950), is that each component of the strain rate tensor is proportional to the corresponding component of σ'_{ij}, i.e.

$$\dot{\varepsilon}_{ij} = \lambda \sigma'_{ij}, \tag{9}$$

where λ is a function of pressure, temperature, σ'_{ij}, etc. Equation 9 is the form of the yield criterion used throughout the literature, and is the basis for further discussion. It is common to refer to Equation 9 as a flow law, although the term is practically synonymous with yield criterion. As a yield criterion, Equation 9

carries with it a connotation of perfect plasticity, that is to say, the yield stress cannot be exceeded. Calling Equation 9 a flow law implies there is a strain rate dependence of the condition of perfect plasticity.

A common form for the flow law for creep of crystalline materials at high temperature, and the one we take for the creep of ice, is

$$\dot{\varepsilon} = Ad^{-p}\sigma^{n}e^{-(E^{*}+PV^{*})/RT}, \tag{10}$$

where P is pressure, or more accurately the mean stress (Equation 2), d is grain size, T is temperature, R is the gas constant, and A, p, n, E^{*}, and V^{*} are flow constants particular to the mechanism, discussed below. Equation 10 is the basis for much of the experimental data that will be given in this paper, so the scalar quantities $\dot{\varepsilon}$ and σ are shown as those appropriate to axisymmetric flow. However, they may be substituted by any strain rate and stress components or reduced quantities as long as they bear the relationship given in the general flow law (Equation 9; i.e. they are resolved along the same direction or formulated in parallel fashion from their respective tensors). Equation 10 applies to the steady state: ε, the magnitude of strain, is not an explicit or implicit variable.

The flow law (Equation 10) is empirically based. Although it includes some fundamental deformation physics (e.g. thermal activation), it was formulated primarily to fit laboratory and field measurements rather than the theory of plasticity. Equation 10 is a scalar representation of a tensor relationship, and one must be careful to avoid ambiguity when it is applied. The stress σ may be a shear stress, an octahedral stress, a differential stress, etc (but not a deviatoric stress because that is only a tensor). As long as the user is specific about the usage and correct in its application, there should be no confusion.

Axisymmetric flow described by Equation 10 is a special case of Equation 9, but it is instructive and useful for field applications to try to generalize Equation 10. There will usually be a loss of accuracy as discussed below, but very often it is beyond our means to carry out experiments in anything but the simplest of geometries. The following exercise is based on Nye (1957), but has been repeated numerous times elsewhere. Paterson (1994) gives a number of similar (but simpler) transformations.

Squaring both sides of Equation 9 and substituting from Equation 5, we have

$$\dot{\varepsilon}_{\text{eff}} = \lambda\tau_{\text{eff}}. \tag{11}$$

The scalar stress dependence must be the same in both Equations 10 and 11. Therefore we can write

$$\dot{\varepsilon} = B\sigma^{n} \tag{12}$$

and

$$\dot{\varepsilon}_{\text{eff}} = D\tau_{\text{eff}}^{n}, \tag{13}$$

where B and D at fixed temperature, pressure, grain size, etc are constants. Combining Equations 11, 13, and 9 we have

$$\lambda = D\tau_{\text{eff}}^{n-1}. \tag{14}$$

If we align σ_{11} with σ as in Equation 6, then σ'_{ij} is given by Equation 8. Likewise, from volume conservation and axisymmetry we have

$$\dot{\varepsilon}_{ij} = \begin{pmatrix} \dot{\varepsilon} & 0 & 0 \\ 0 & -\dot{\varepsilon}/2 & 0 \\ 0 & 0 & -\dot{\varepsilon}/2 \end{pmatrix}. \tag{15}$$

Thus, from Equations 5 and 8,

$$\tau_{\text{eff}} = (1/3)^{1/2}\sigma \tag{16}$$

and from Equations 5 and 15,

$$\dot{\varepsilon}_{\text{eff}} = (3^{1/2}/2)\dot{\varepsilon}. \tag{17}$$

From Equations 12, 13, 16, and 17,

$$D = 3^{(n+1)/2}B/2. \tag{18}$$

Substituting Equations 16 and 18 into 14 allows us to calculate λ and therefore the general flow (Equation 9) at any conditions. Note that, because this calculation applies the Tresca yield criterion (Equation 12) to the more accurate von Mises formulation (Equation 13), λ calculated in this manner will be slightly less accurate than λ determined by the more complex but direct experiment wherein a more general state of stress is imposed.

Viscosity

It is common in planetary dynamics to speak of viscosity of non-Newtonian materials ($n \neq 1$ in Equation 10) even though the term is not fully descriptive of rheology. As long as the term is used properly, i.e. if σ or $\dot{\varepsilon}$ is specified, one may speak of the effective viscosity, η_{eff}, of a material, where

$$\eta_{\text{eff}} = \sigma/(3\dot{\varepsilon}). \tag{19}$$

The factor of 3 in the denominator results from the fact that the flow is axisymmetric and divergent rather than along straight, parallel lines (e.g. Macosko 1994, p. 94).

RHEOLOGY OF WATER ICE

Terrestrial vs Planetary

The flow of ice caps and glaciers on Earth has inspired much field and laboratory measurement and theoretical development related to ice rheology. Excellent reviews of this work exist (Alley 1992; Budd & Jacka 1989; Goodman et al 1981; Kamb 1964; Paterson 1994; Petrenko & Whitworth 1999; Weertman 1973, 1983). Most extraterrestrial ice exists at conditions considerably beyond the range of reasonable extrapolation of terrestrial knowledge, so interest in planetary ice required new investigations. The treatment to date of planetary ice rheology has been far less thorough than that of terrestrial. The rheology of ice at planetary conditions reviewed here is based on data compiled by Durham et al (1997), with the addition of important new results on grain-size-sensitive (GSS) creep in ice I by Goldsby & Kohlstedt (1997, 2001). This review is limited to water ice as the volatile component of interest. Limited information can be found on the flow of other ices at planetary conditions: $NH_3 + H_2O$ (Durham et al 1993), methane clathrate (Stern et al 1996), CO_2 (Clark & Mullin 1976, Durham et al 1999), and N_2 and CH_4 (reviewed by Eluszkiewicz & Stevenson 1990).

Mechanisms of Deformation

To this point we have treated solids as continua, but in fact it is their internal structure that defines how ductile flow is affected at the lattice scale. Deformation is carried out by mechanisms that involve the coordinated motion of crystal defects, such as point defects (vacancies and interstitials), line defects (dislocations), and planar defects (subgrain boundaries, grain boundaries) (e.g. see Poirier 1985). Considering that the motion of each type of defect has its own dependence on external conditions (σ, T, P, etc), and that impurities, second phases, and such processes as melting and phase change can be involved, many deformation mechanisms are potentially available to a material. It is also important to appreciate that at $T > 0$ K, all mechanisms operate, but that the relative amount of deformation contributed by each changes as external conditions change. At a given set of conditions, therefore, one mechanism will dominate the rheology, i.e. contribute the majority of the strain rate. As conditions change, different mechanisms will dominate.

The concept of a dominant mechanism is particularly important with respect to the rheology of planetary ices (and of other geological materials) because the range of strain rates pertinent to the planets is very broad—from $\dot{\varepsilon} = 10^{-14}$ s^{-1} or slower in, say, the convecting interior of a Ganymede-type body to explosive rates of $\dot{\varepsilon} > 1$ s^{-1} during meteoritic impact. "Quasi-static" laboratory experiments intended to constrain the slower geologic processes are most commonly in the range of $10^{-7} < \dot{\varepsilon} < 10^{-4}$ s^{-1}, giving only a narrow perspective on the planetary settings. It is thus necessary for the planetary application to remain alert to the

possibility of transitioning to a regime dominated by a flow mechanism other than that which dominates under laboratory conditions (Paterson 1987). Laboratory-measured strength is generally an upper bound when extrapolated to lower strain rates and a lower bound when extrapolated to higher rates.

Each mechanism can be described constitutively by an equation of the general form of Equation 9, with the factor λ embodying the dependence of strain rate on all relevant environmental conditions. Table 1 lists the flow parameters (Equation 10) for all laboratory-measured deformation mechanisms for water ice I and for each of the several high-pressure polymorphs of water.

Independent vs Dependent Mechanisms

As discussed above, in any material under stress, many mechanisms of deformation can and do operate. Langdon & Mohamed (1977) distinguished two ways that these deformation mechanisms interact. When several mechanisms are acting simultaneously, they are termed independent and the total strain rate in the material is the simple sum of the strain rate contributed by each mechanism (Figure 1*a*). Considering for simplicity two mechanisms *a* and *b*, if each contributes strain rates $\dot{\varepsilon}_a$ and $\dot{\varepsilon}_b$, then

$$\dot{\varepsilon}_{\text{tot}} = \dot{\varepsilon}_a + \dot{\varepsilon}_b. \tag{20}$$

At fixed temperature, the mechanism with higher stress sensitivity will dominate at higher values of stress (Figure 1*a*). In other words, if the two mechanisms act independently and are described by n_a and n_b (Equation 10), respectively, where $n_b > n_a$, then at higher stresses $\dot{\varepsilon}_b > \dot{\varepsilon}_a$.

Situations arise, however, where mechanisms *a* and *b* cannot operate independently (Langdon 1996, Langdon & Mohamed 1977, Raj & Ghosh 1981), including in water ice (Goldsby & Kohlstedt 1997, 2001). In such a case, where $n_b > n_a$, then at higher stresses $\dot{\varepsilon}_b < \dot{\varepsilon}_a$ (Figure 1*b*), and it can be shown that

$$(\dot{\varepsilon}_{\text{tot}})^{-1} = (\dot{\varepsilon}_a)^{-1} + (\dot{\varepsilon}_b)^{-1}. \tag{21}$$

Langdon & Mohamed (1977) asserted that the fundamental requirement behind Equation 21 is that in any increment of strain, the amount of strain contributed by each mechanism must equal the total strain, i.e.

$$\varepsilon_{\text{tot}} = \varepsilon_a = \varepsilon_b. \tag{22}$$

We show below that this may in fact not be a necessary condition for Equation 21.

Langdon & Mohamed (1977) termed mechanisms *a* and *b* sequential. We prefer the term dependent because there are examples of sequential submechanisms *a* and *b* within a given mechanism that do not obey Equation 21. Additionally, there are examples of mechanisms *a* and *b* that do not act in sequence, but that together obey Equation 22 and therefore Equation 21. An example of the former is dislocation creep, a mechanism that can be thought of as the sequential operation of dislocation

TABLE 1 Rheological constants for water ice used in Equation 10

Phase	Creep Regime	$\log A$ ($MPa^{-n}\ m^{p}\ s^{-1}$)	p	n	$E^{\star}$ (kJ/mole)	$V^{\star}$ (cm^3/mole)	Reference
Ice I	Dislocation creep						
	>258 K	28.8	0	4	181	-13^{a}	Goldsby & Kohlstedt (2001)
	Regime A (258-240 K)	11.8 ± 0.4	0	4.0 ± 0.6	91 ± 2	-13^{a}	Durham et al (1992)
	Regime B (240 K -[c])	5.1 ± 0.03	0	4.0 ± 0.1	61 ± 2	-13 ± 3	Durham et al (1992)
	Regime C ([c])	-3.8^{b}	0	6.0 ± 0.4	39 ± 5	-13^{a}	Durham et al (1997)
Ice I	Grain-size-sensitive creep						
	GBS-limited (>255)	26.5	1.4	1.8	192	-13^{a}	Goldsby & Kohlstedt (2001)
	GBS-limited (<255)	−2.4	1.4	1.8	49	-13^{a}	Goldsby & Kohlstedt (2001), Durham et al (2001)
Ice I	Basal slip-limited GBS	7.74	0	2.4	60	-13^{a}	Goldsby & Kohlstedt (2001)
Ice II	<220 K	1.84 ± 0.27	0	5.3 ± 0.1	55 ± 2	7 ± 1	Durham et al (1988)
Ice II	≥220 K	11.7 ± 1.6	0	5.2 ± 0.3	98 ± 8	4 ± 4	Durham et al (1988)
Ice III	<230 K	13.3 ± 1.5	0	6.3 ± 0.4	103 ± 8	0^{a}	Durham et al (1988)
Ice III	≥230 K	26.4 ± 4.8	0	4.3 ± 1.2	151 ± 21	0^{a}	Durham et al (1988)
Ice V		23^{b}	0	6 ± 0.7	136 ± 38	29 ± 8	Durham et al (1996)
Ice VI	<250 K	6.7^{b}	0	4.5 ± 0.2	66 ± 4	11 ± 6	Durham et al (1996)
Ice VI	≥250 K	6.7^{a}	0	4.5^{a}	110 ± 20	11^{a}	Durham et al (1996)
Ice V		−1.27	0	2.7 ± 1	32.4 ± 9.6	10.1 ± 9	Sotin and Poirier (1987)
Ice VI		−10.6	0	1.93 ± 0.02	28.5 ± 1	8.1 ± 0.8	Sotin et al (1985)

Uncertainties are 1 standard deviation, except as noted.
[a]Estimate; not measured.
[b]Uncertainty included in those of n, $E^{\star}$, and $V^{\star}$.
[c]Boundary between Regimes B and C depends on temperature and strain rate.

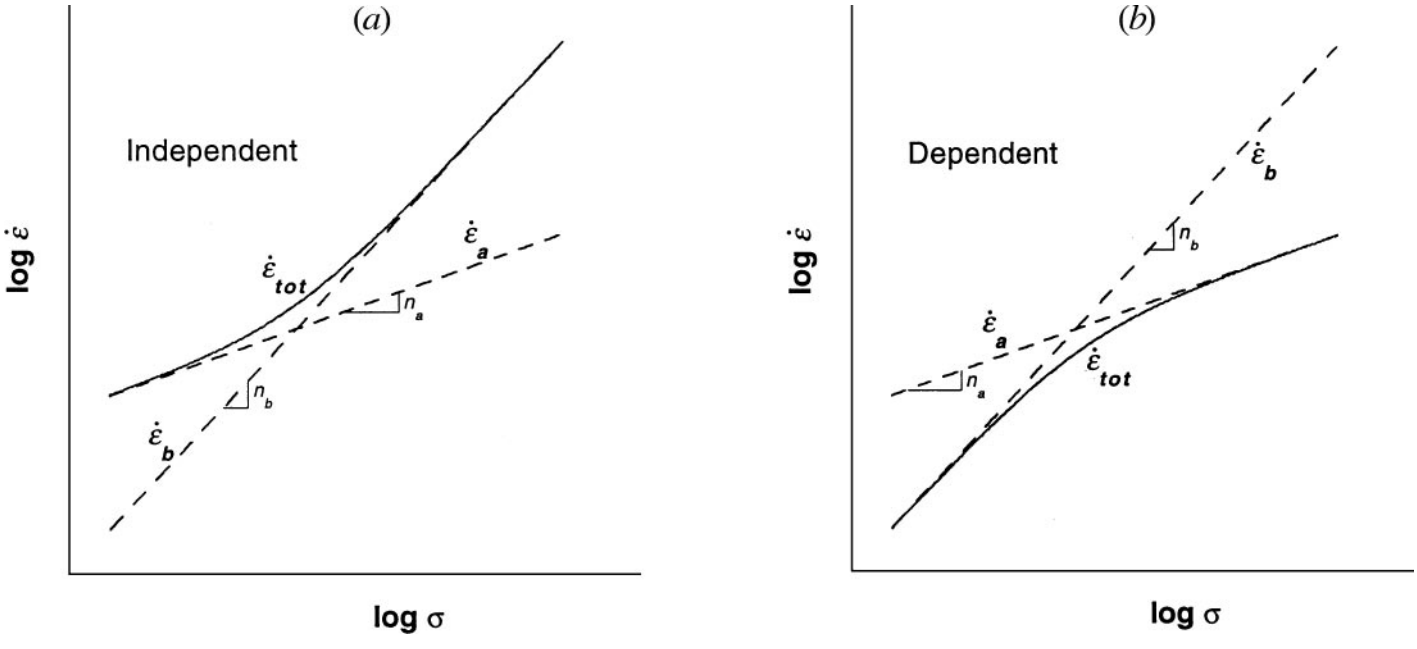

Figure 1 The rheological manifestation at fixed temperature of two mechanisms of deformation that operate (*a*) independently and (*b*) dependently. In the former case, the strain rates of mechanisms *a* and *b* (dashed lines) add in a simple way (Equation 20) to produce a resultant log $\dot{\varepsilon}$–log σ curve that is concave upward. In the latter case (*b*), the mechanisms combine according to Equation 21 to produce a curve that is concave downward. The stress exponents (Equation 10) for the two mechanisms, n_a and n_b, are the slopes of the two dashed lines. All independent mechanisms behave as in *a*, but not all dependent mechanisms behave as in *b*. See text for details.

glide limited by dislocation climb. Generally in an increment of strain, $\varepsilon_{\text{glide}} \gg \varepsilon_{\text{climb}}$ (Weertman 1968), so the sequential substeps of dislocation creep cannot obey Equation 21. An example of the latter is given by Raj & Ghosh (1981), where, in a polycrystalline sample with bimodal grain sizes, different mechanisms operate in large and small grains. The mechanisms act simultaneously, but strain continuity in the aggregate requires Equation 22, and the experimental data in fact follow Equation 21, i.e. a curve like that in Figure 1*b*. For the case of water ice, Goldsby & Kohlstedt (1997, 2001) fit the transition from $n = 1.8$ to $n = 2.4$ (Table 1) to a curve of the form in Figure 1*b*. Possible interpretations of this behavior are discussed in the following section. The point here is that one should avoid the thought that Equation 21 automatically means sequential operation and dependent mechanisms, and vice versa. There has been some confusion over this matter in published work (Poirier 1985).

Ice I

Deformation experiments on polycrystalline ice I have covered conditions that include most of the T, P range of interest to satellites of the outer solar system (Durham et al 1992). The regime most easily encountered at laboratory conditions is that of dislocation creep, which is characterized by a high stress dependence, $n \geq 3$ in Equation 10, and mechanistically involves the glide motion of dislocations accommodated by dislocation climb. In addition, ice I is one of the few materials for which well-resolved rheological data exist on GSS creep, in which grain boundaries themselves act as slip planes, short cuts for diffusion, and sources and sinks of diffusing species. GSS creep is characterized by a lower stress dependence, $n \leq 2$, and an inverse dependence on grain size, $p > 0$ in Equation 10.

For detailed descriptions of defects in ice and the mechanistic details of their role during deformation (with emphasis on terrestrial conditions) the reader is referred to Petrenko & Whitworth (1999).

Deformation Map of Ice I It is useful to compare the complex relationships between deformation mechanisms in ice visually on a deformation map (Frost & Ashby 1982, Goodman et al 1981), in which loci of constant strain rate are plotted as contour lines on appropriate axes. The dominant mechanism at any point is that which contributes the most strain rate, and the map can then be subdivided into areas of dominance by each mechanism. D Goldsby & D Kohlstedt (personal communication) have recently published an updated version of the deformation map for ice I (Figure 2). In order to plot in two dimensions σ vs T in Figure 2, the variables P and grain size d are held constant. The effect of P within the dislocation creep field has been measured and is fairly small, characterized by $V^* = -13$ cm^3/mol. This corresponds to an increase in strain rate by a factor of about 5 from $0 > P > 200$ MPa (the width of the ice I stability field) (Figure 3) at $T = 200$ K. The pressure effect is likely to be similar for all mechanisms that are limited by volume or grain boundary diffusion (dislocation creep, diffusion

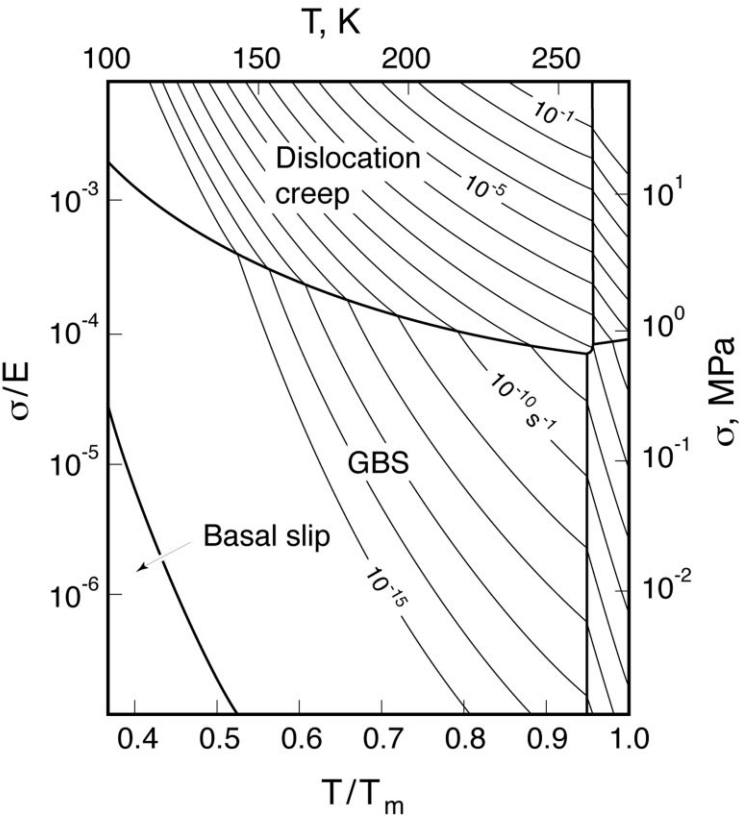

Figure 2 Deformation map for polycrystalline ice of 1-mm grain size. Axes are temperature T and differential stress σ, also given in coordinates normalized by melting temperature $T_m = 273$ K and Youngs modulus $E = 9.3$ GPa, respectively. At any given set of (σ,T) conditions, one mechanism of deformation will dominate the strain rate. Dislocation creep, grain-boundary sliding (GBS, also called grain-size-sensitive or GSS creep), and basal slip dominate in the fields so labeled. Lighter lines are contours of constant strain rate spaced at intervals of one order of magnitude. Calculations are based on Equation 10 and the flow constants in Table 1. Dislocation creep is combined as independent (Equation 20) with respect to the pair of mechanisms basal slip and GBS, which themselves are combined as dependent (Equation 21). See text for further details. (From D Goldsby & D Kohlstedt, personal communication.)

creep, GSS creep). The effect of grain size is more substantial; changes in grain size over a reasonable range are sufficient to change the overall appearance of the deformation map. The relationship between GSS creep and dislocation creep is of special interest in this review and is discussed more below.

Neither dislocation creep nor GSS creep follows a single constitutive law across the range of external conditions. Cast into the form of the empirical creep law

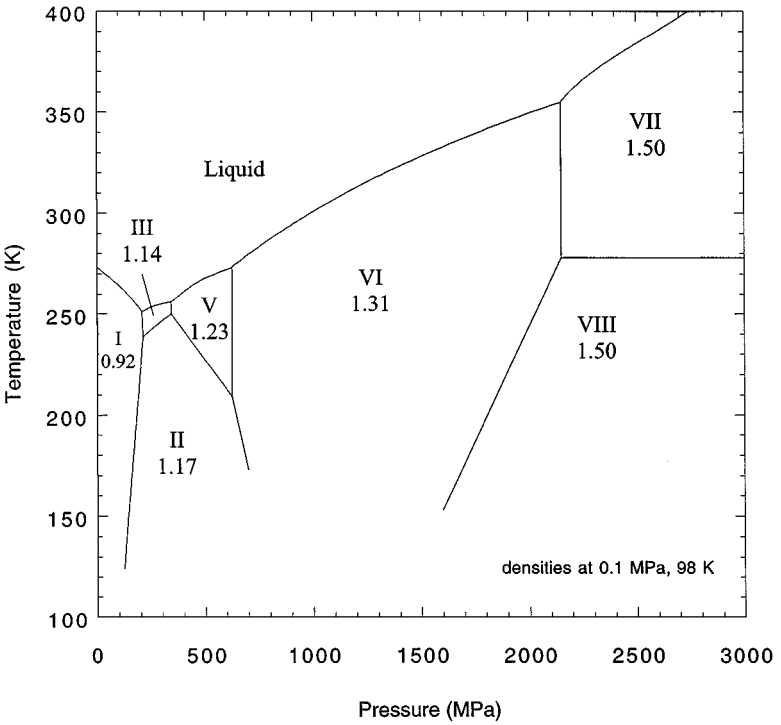

Figure 3 Phase diagram for water ice. Data from Fletcher (1970) and Bridgman (1912).

(Equation 10), the observations require at least three different sets of flow parameters within dislocation creep and two within GSS creep. There may be more. The reason for this is that the coordinated micromechanical subprocesses that together are manifested as, say, dislocation creep have unique dependencies on σ, T, etc. For the most part, those individual dependencies are not known. As knowledge advances, Equation 10 and Table 1 will presumably be replaced by more accurate formulations.

Dislocation Creep Regimes A and B The activation energy E^* for dislocation creep regime B is 61 kJ/mol. This suggests that deformation is limited by self-diffusion, which has an activation energy of about 60 kJ/mol (Weertman 1983). The same value holds for single crystals deformed right up to melting (see Petrenko & Whitworth 1999). In polycrystalline ice, however, the temperature sensitivity accelerates at warm temperatures in a way that cannot be described by simple thermal activation (Equation 10), which suggests to many that grain-surface "premelting" (Dash et al 1995) may occur in polycrystalline material. Very close to the melting temperature, pressure melting may also occur at local stress concentrations, such as at grain corners and edges. For the purposes of the deformation

map, Goldsby & Kohlstedt (2001) select a value of 181 kJ/mol to describe the flow. The dislocation creep regime A identified by Kirby et al (1987) at $240 < T < 256$ K with $E^* = 91$ kJ/mol suggests that premelting extends to 240 K. The value of n in this high-temperature regime is in dispute. A value of $n = 3$, the so-called Glen law (Glen 1955) has long been accepted as an accurate description of the flow of ice to temperatures at least as low as 240 K, but Peltier et al (2000) have recently shown that better agreement to laboratory and field data comes by considering a two-mechanism model of $n = 4$ dislocation creep plus $n = 1.8$ GSS, according to the parameters in Table 1.

Dislocation Creep Regime C At low temperature and high differential stress, a third regime, C, appears, characterized by $n = 6$ and $E^* = 31$ kJ/mole (Table 1). It is based entirely on measurements made in our laboratory (Durham et al 1983, 1992, 1993; Kirby et al 1987). D Goldsby (personal communication) has recently suggested that the behavior we observed was influenced by distributed cataclasis, noting the relatively poor reproducibility of our data at $T < 195$ K and the fact that differential stresses reached and sometimes exceeded the confining pressure (usually 50 MPa). We note further that this suggestion is consistent with our unpublished observations of a transition in macroscopic sample appearance at 195–180 K. At warmer temperatures, the material after deformation testing is clear and transparent; at and below the transition, the sample appearance becomes mottled and increasingly cloudy, which may suggest a departure from pure ductility (Rist & Murrell 1994). The hypothesis of distributed microfracturing is ordinarily easy to test in rock mechanics because of its first-order dependence on confining pressure (higher pressure will cause strength to increase). Ice I presents a special problem, however, due to the proximity of test conditions to the ice I $\rightarrow$ II phase transformation. The $\sim$20% volume decrease that accompanies that transformation has a demonstrable effect on the apparent rheology of ice I (Durham et al 1983). One tenuous regime C experiment at $P = 80$ MPa gave the same strength value as tests at 50 MPa, but the existence of the ice I $\rightarrow$ II transition at about 150 MPa (Figure 3) leaves open the possibility that local mean stresses caused local transformation and lowered strength. The experimental problem is further complicated by the fact that it is the maximum stress σ_{11}, not the mean stress σ_m that seems to determine the onset of the I $\rightarrow$ II transition (Kirby et al 1992).

Further progress in confirming the veracity of regime C probably requires high-strain testing at $\dot{\varepsilon} < 10^{-8}\,\mathrm{s}^{-1}$, so it is unlikely to occur soon. Regarding its relevance to the icy moons, regime C can be mostly ignored. The transition between regimes B and C tends toward lower temperatures at lower stresses. If this trend continues to planetary stresses <1 MPa, then regime C will dominate over regime B only at near-surface temperatures of <120 K, and then only at $\dot{\varepsilon} < 10^{-20}\,\mathrm{s}^{-1}$.

Grain-Size-Sensitive Creep Goldsby & Kohlstedt (1997), who first observed the GSS creep mechanism experimentally in ice at planetary temperatures, suggested the $n = 1.8$ behavior was a grain boundary sliding (GBS)-limited mechanism on

the basis of similarities to mechanisms of superplasticity in metals and ceramics. Durham et al (2001), confirming that the Goldsby & Kohlstedt (1997) flow law described a volume-conservative mechanism, preferred the less-specific designation GSS, which we take here. At lower temperatures and strain rates, Goldsby & Kohlstedt (1997) found the behavior grading to $n = 2.4$ in the manner of Figure 1*b*. The $n = 2.4$ rheology matched that of single crystals oriented for easy slip on the basal or *c* plane (see Goldsby & Kohlstedt 2001), so Goldsby & Kohlstedt surmised that GBS combined with basal slip in dependent fashion accounted for their GSS mechanism. While neither basal slip nor GBS alone is sufficient for general deformation, together they are sufficient, or at least nearly enough sufficient that other accommodating submechanisms do not significantly affect the creep law. Basal dislocations piling up at grain boundaries can be relieved by rigid sliding at grain boundaries, or geometric barriers to rigid sliding can be eliminated by the slip of basal dislocations. Grain-size sensitivity appears where GBS controls the creep rate, but not where basal slip controls (Table 1). Equation 21 is consistent with such a mechanism, where control is passed from one submechanism to the other, and does not require Equation 22. It may be argued that given the nature of the operation of the two particular submechanisms here, Equation 22 does in fact apply (D Goldsby, personal communication). Further laboratory and microstructural observations are required to resolve whether or not Equation 22 applies to GSS creep in ice.

Ice I Plus Particulates

Hard particulates of varying size and composition do not have a profound effect on the steady state strength of ice I (Durham et al 1992). Particulates have variable effects at terrestrial conditions where grain boundaries are mobile and brittle fracture occurs (Baker & Gerberich 1979, Hooke et al 1972, Nayar et al 1971), but at cooler temperatures in the ductile field, the effect of particulates is a hardening caused mainly by increased tortuosity of flow paths around particles and viscous drag of flowing ice at particulate surfaces. There is no indication from experiment that hardening by pinning dislocations, as in dispersion hardening (see Durham et al 1992) is an important process in ice I at planetary conditions. At warm temperatures, particulate pinning of grain boundaries can soften ice by impeding grain growth, thus retaining creep within the GSS regime (Baker & Gerberich 1979, Hooke et al 1972). For the dislocation creep regime, Durham et al (1992) found that for ice I mixed with hard particulates at volume fraction $0 \leq \phi \leq 0.56$ and $142 \leq T \leq 223$ K, the rheology follows the relationship

$$\sigma_{\text{ice I + particulates}}(P, T, \dot{\varepsilon}) = \sigma_{\text{pure ice}}(P, T, \dot{\varepsilon}) \exp(b\phi), \tag{23}$$

where $b \approx 2$. At $\phi = 0.56$, which is near the theoretical packing limit for equal-sized spheres, the hardening is roughly a factor of 3 to 4 in σ, or about two orders of magnitude is η_{eff} for $n = 4$ rheology.

Ices II, III, V, and VI

Figure 3 shows a portion of the phase diagram for water. The rheologies of all the planetary water ice phases except VII and VIII have been measured, although at limited conditions and with considerably higher uncertainties than for ice I (Durham et al 1988, 1996; Echelmeyer & Kamb 1986; Poirier et al 1981; Sotin et al 1985; Sotin & Poirier 1987). The generally high values of n in Table 1 suggest dislocation creep is the dominant mechanism. Bennett et al (1997) observed fabric in ice II consistent with deformation by dislocation motion, with the primary slip system being glide on prism planes in the [0001] direction. Sotin et al (1985) measured a low value $n = 1.9$ for ice VI using the sapphire anvil cell, although the magnitude of η_{eff} at laboratory stresses were close to those observed by Durham et al (1996), who measured $n = 4.5$ in a triaxial deformation apparatus. There are at least two possible explanations for the disagreement. The first is that the rheology observed in both laboratories was the same, but systematic error and measurement imprecision in these difficult experiments resulted in inconsistent interpretations. The second is that the rheology observed in the sapphire anvil was GSS, and that η_{eff} under the two different mechanisms at laboratory conditions happened to be nearly coincident, just as they are for ice I. Sotin et al (1985) did not specify the grain size of their material, although given the relatively small volume of their cell, it is likely to have been small. They did acknowledge that their low value of n was highly unusual in solids tested at such high stresses. There is also disagreement between laboratories over η_{eff} for ice V. Under identical laboratory conditions, the effective viscosity of ice V measured in the sapphire anvil is about three orders of magnitude higher than that measured in the triaxial apparatus. The matter has been considered at length but has not been resolved (Durham et al 1997).

The (P, T) field of ice III stability is quite small (Figure 3), ordinarily too narrow to allow good resolution of some of its flow parameters. However, it is possible to measure E^* with good precision because of a profound metastability of ice III in the ice II stability field (Bridgman 1912, Durham et al 1988), even allowing identification of a mechanism change in ice III near 230 K (Table 1), deep within the ice II stability field.

The lack of well-resolved constitutive relationships for mechanisms other than dislocation creep leaves us with flow laws that are safely used only as upper bounds on the strength of icy planetary interiors. It is likely, based on repeated experience with other oxides and metals (and ice I), that grain boundary effects will influence rheological behavior at low stress. The only question is how low a stress. The $n = 1.9$ rheology for ice VI mentioned above is a possible sign of such creep. Stern et al (1997) were able to create samples of fine-grained ice II (grain size near 10–15 μm), which did show extreme weakness, but the results were impossible to deconvolute due to the simultaneous operation of the ice I $\rightarrow$ II phase transformation. There is one tenuous link to quantification. If the anomalously high strength of ice V measured by Sotin & Poirier (1987) was the result of systematic error in the measurement of σ in the sapphire anvil cell,

and if the ice VI results were affected by the same problem without affecting the observed $n = 1.9$, then we can infer that the effective viscosity of VI in GSS creep at lab conditions is about three orders of magnitude lower than that for dislocation creep.

Figure 4 is a style of deformation map comparing the rheologies of the several phases on the ice phase diagram at a "planetary" strain rate of $10^{-13}\,s^{-1}$, calculated from the flow constants in Table 1. Ice II at lab conditions is the strongest of the phases, and ice III the weakest by a considerable margin. Extrapolated to planetary rates, the high n value of ice V brings its strength closer to that of ice II.

RHEOLOGICAL COMPLEXITIES

Dislocation Creep Vs Grain-Size-Sensitive Creep

From the flow laws for ice I, the possibility that ice I is deforming in the GSS creep regime in natural settings is quite plausible. Many researchers have come to this conclusion already (McKinnon 1999, Nye 2000, Pappalardo et al 1998b, Peltier et al 2000). At 1-mm grain size (Figure 2), GSS creep will dominate at stresses below a few 0.1 MPa for most temperatures. The boundary between GSS

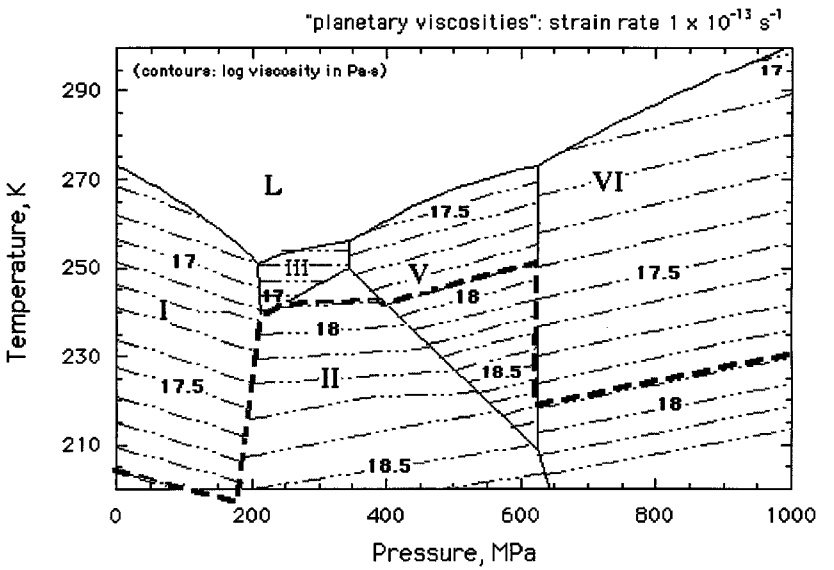

Figure 4 Deformation map comparing the rheologies of several of the high-pressure ice phases, superimposed on the phase diagram for water. Contoured in each phase field is the effective viscosity, η_{eff}, based on Equations 10 and 19 and the flow constants in Table 1, calculated at a "planetary" strain rate of $10^{-13}\,s^{-1}$. The heavy dashed line traces the $\eta_{\text{eff}} = 10^{-17.9}$ Pa · s contour across the map. (From Durham et al 1997.)

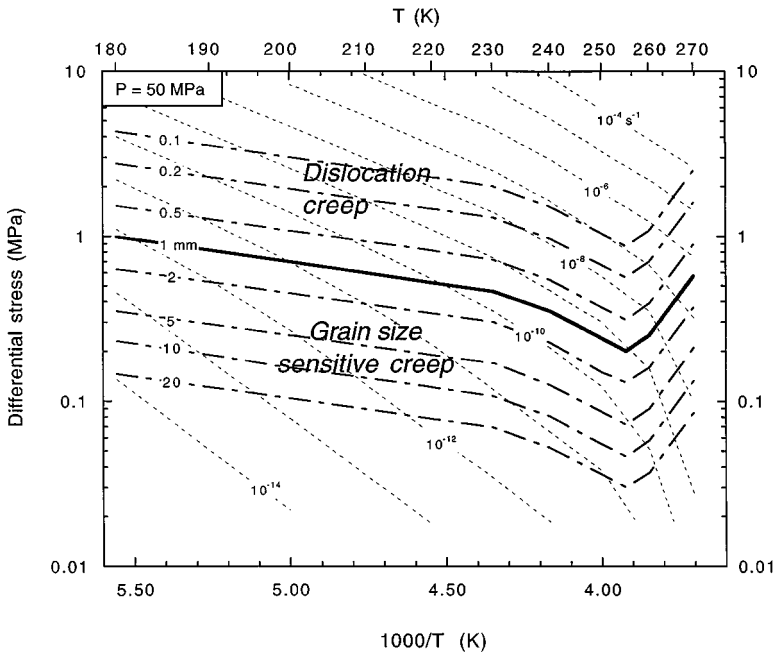

Figure 5 Warm-temperature portion of the deformation map in Figure 2 showing how the boundary between the fields of dominance of dislocation creep and grain-size-sensitive creep (GSS) moves with grain size. Note that the horizontal scales are now linear in $1/T$. Short-dashed lines are strain-rate contours, as in Figure 2. GSS creep produces higher strain rates at smaller grain sizes, whereas dislocation creep is unaffected by a change in grain size (Equation 10, Table 1). The heavy solid line is the boundary between dislocation creep dominance and GSS creep dominance at 1-mm grain size, as in Figure 2. The GSS field expands at the expense of dislocation creep as grain size decreases, and contracts as grain size increases, as shown by the long/short dashed lines (WB Durham, LA Stern, SH Kirby, submitted for publication).

and dislocation creep is itself GSS, of course, as shown in Figure 5. Geologic time, however, favors both low stresses and grain growth. These act at cross purposes with respect to dominance of GSS creep over dislocation creep. Thus, to understand rheology in natural settings, it is important to understand processes that influence grain size.

Grain size is probably not a free variable, despite the form of the creep law Equation 10. Thermodynamic forces associated with curved grain boundaries and intracrystalline defects drive processes of normal grain growth and recrystallization that lead to grain-size increase or reduction. The process is ongoing during deformation, because defects are constantly being generated, and is termed dynamic recrystallization. In the geologic view, that is, over very long times and very large strains, dynamic recrystallization can be expected to lead to a prescribed grain

size [for a general review of these topics, see Poirier (1985)]. The key rheological question is, does the grain size balance, once achieved, put the material in the GSS creep field or the dislocation creep field?

Normal grain growth proceeds at a temperature-dependent rate K according to

$$d^2 - d_0^2 = Kt$$
$$K = K_0 e^{-Q/RT}, \tag{24}$$

where d_0 is the grain size at time $t = 0$ and K_0 and Q are constants (e.g. Porter & Easterling 1992). The rate K derived from limited laboratory studies (Arena et al 1997) and from grain size vs age and temperature observations in terrestrial ice sheets (De La Chapelle et al 1998, Duval & Lliboutry 1985, Gow 1969) is roughly that identified by Gow (1969) as $K_0 = 5.9$ mm$^2 \cdot$s^{-1} and $Q = 48.6$ kJ/mol. If normal growth acts alone, then in the actively convecting portion of a Europa ice shell with a mean $T = 235$ K (Pappalardo et al 1998b), grain diameters will reach at least several millimeters within a few thousand years, and GSS creep will slow to rates below those of dislocation creep.

It has been widely observed that dynamic recrystallization leads to a simple relationship between grain size (or subgrain size) and stress, independent of temperature and other variables. Thus,

$$d = A\sigma^{-m} \tag{25}$$

where $m = 1$ or slightly larger and A is a material constant. In geology, this particular relationship provides workers with a powerful paleopiezometer (Twiss 1977), given a rock sample for which there is evidence that the current grain size is the result of dynamic recrystallization. Equation 25 is widely used, perhaps because of its appealing simplicity, but it is mainly empirical and its theoretical support is shaky at best (Poirier 1985). A closer examination of the dynamic balance between processes of recrystallization and the generation of dislocations during creep shows that A in Equation 25 is generally temperature sensitive and potentially dependent on the stress exponent n in the creep law (Equation 10) (Derby 1990, Derby & Ashby 1987, Shimizu 1998). Among studies where Equation 25 has been applied to dynamic recrystallization in ice is a compilation by Jacka & Li (1994), who found that $m = 3$ for ice at very warm temperatures ($>$263 K). de la Chapelle et al (1998) used Equation 25 with an assumed value of $m = 1$ at cooler temperatures along with grain-size measurements in ice cores to estimate strain rates in terrestrial ice sheets. McKinnon (1999) used Equation 25 in reverse (as discussed below), along with reasonable strain rates for deforming ice in the Europan ice shell, to calculate that ice grain size should be $<$1 mm at 260 K, implying a GSS rheology (Figure 5).

Deformation by dislocation creep will generate dislocations and other defects that will drive grain size smaller, pushing rheology toward the GSS field. Conversely, if GSS is incapable of generating dislocations, then material deforming

purely by GSS will experience only normal grain growth, driving rheology toward the dislocation creep field. de Bresser et al (1998) suggested that the rheological balance thus reached between GSS and dislocation creep must be very close to that at the boundary between the two regimes, so that the steady state grain size would be approximately that calculated by equating the two flow laws (Equation 10) for dislocation creep (subscripts disloc) and GSS (subscripts GSS):

$$d = (A_{GSS}/A_{disloc})^{1/p} e^{(Q_{disloc} - Q_{GSS})/pRT} \sigma^{-(n_{disloc} - n_{GSS})/p}, \qquad (26)$$

where $Q \equiv E^* + PV^*$. The de Bresser et al (1998) hypothesis currently lacks a detailed microphysical basis, although there is remarkably strong support for Equation 26 in laboratory data on deformed olivine and calcite (de Bresser et al 2001).

It should be emphasized that the preceding discussion applies to pure ice. The thought that grain size is deterministic and that its rheology does not require additional observational data must be an attractive one, both to modelers of planetary processes and to experimentalists. It is clear from terrestrial observations, however, that chemical impurities and dust cause a distinct slowing of normal grain growth (Alley et al 1986; Alley & Woods 1996; Thorsteinsson et al 1995, 1997). When two deforming phases are present, processes can become considerably more complex. There is ample terrestrial evidence for localized shear zones indicative of GSS creep-related instabilities, for example.

A similar situation should exist in planetary settings. On the cold surfaces of the large icy moons of Jupiter and beyond, where temperatures are near 100 K, grain growth of H_2O ice will be slow. Figure 2 suggests that GSS mechanisms will dominate, assuming values of $\sigma < 1$ MPa. At warmer interior temperatures, however, the range of domination of dislocation creep reaches to lower stresses and at the same time grain sizes will be larger, further widening the dislocation creep field (Figure 5). It seems that accurate modeling of flow on large celestial bodies from Earth to Europa requires consideration of both flow mechanisms.

The Brittle Field

The strength of the outermost layers of an icy moon may be influenced by the brittle properties of ice. In the terminology of the previous section, the transition from ductile to brittle behavior occurs in the near-surface region, where differential stress is comparable to lithostatic pressure so that volume nonconservative mechanisms are allowed to operate. Ductile mechanisms of deformation are typically more temperature sensitive than brittle mechanisms, so the low temperature of planetary surfaces also favors brittle deformation. Where the crustal material is intact, perhaps as on younger surfaces such as Europa's, brittle behavior involves creation of new fracture surfaces. Older solar system surfaces are probably laced with fractures from such processes as meteoritic activity, and are therefore weaker. The relevant brittle behavior in that case is frictional sliding.

Understanding intact planetary crusts is currently beyond our capabilities. Interpretation of brittle processes even on our own planet is difficult, because the tensile strength of rock is notoriously scale-dependent and strongly affected by local structural and chemical heterogeneities, and is therefore only weakly constrained by results of laboratory-scale testing. In fact, a similar scaling argument, that brittle strength tends to decrease with increasing sample volume (for a review, see Paterson 1978) strongly suggests that at wavelengths relevant to planetary landforms, intact ice cannot exist, even on Europa. It is much easier to model planetary surfaces if one takes the view that they come prefaulted. For the interested reader, there has been extensive study of the brittle-to-ductile transition in ice at terrestrial temperatures (e.g. see Rist & Murrell 1994) as well as some work at planetary temperatures (Kirby et al 1987).

In the case of a prefaulted crust, brittle behavior is regulated by frictional properties, which are less scale dependent and for which there is sufficient laboratory data to draw a rudimentary strength map for the uppermost layers of an icy moon. Frictional strength depends strongly on pressure but only weakly on temperature, and so increases with depth. Ductile strength depends mainly on temperature, and so decreases with depth. Plotting both these trends as strength vs depth, assuming a reasonable geothermal gradient (and because ductile strength is strain-rate sensitive, also fixing strain rate) generates another style of deformation map (Figure 6). We have already discussed the flow laws for ice I. The curves for brittle strength in Figure 6 are based on measurements by Beeman et al (1988) for the frictional strength on preexisting faults. The coefficient of friction, defined as the shear strength of a fault divided by the stress normal to the fault, is $\mu = 0.55$ at normal stresses below 20 MPa, and drops to 0.20 at higher normal stresses. On the basis of Figure 6, the depth of the brittle crust on Ganymede under extensional conditions should be approximately 10 km.

Preferred Crystallographic Orientation

Isotropic polycrystalline ice, that is, polycrystalline ice whose grains are randomly oriented with respect to one another, can develop a preferred crystallographic orientation during ductile strain. Preferred crystallographic orientation (called fabric by geologists and texture by metallurgists) is a common rheological effect in dislocation creep that is traceable to the existence of favored slip planes and slip directions in the crystal lattice. Just as a deck of playing cards compressed from the ends will slip and rotate away from the direction of compression, so grains of ice I in compression will tend to rotate during deformation such that *c* axes, normal to the weak basal slip plane, will rotate toward the compression direction. The pattern of preferred orientation depends on the state of stress (e.g. Azuma 1994), and the result in some cases is that the strength of the aggregate will be significantly lower than that before the preferred orientation developed. The softening effect, often called tertiary creep (to distinguish it from primary creep, which is the initial strain-dependent inelastic response to load change, and secondary creep, which is

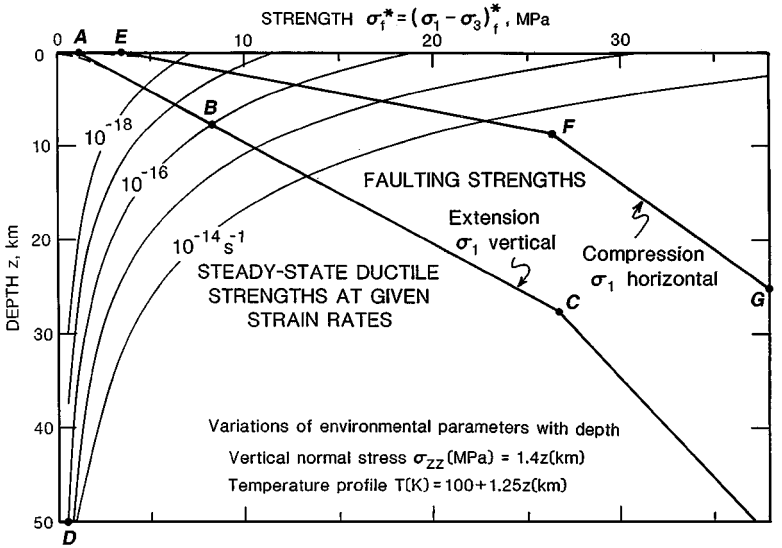

Figure 6 Strength of the Ganymede lithosphere, plotted as maximum differential stress vs depth, assuming the pressure and temperature gradients indicated. Lighter curves show the ductile strength (labeled with strain rate because ductile strength is strain-rate sensitive). The ductile strength curves are calculated from Equation 10 and the flow parameters in Table 1. The deformation regime is B. The heavier curves show the frictional strength of ice, based on the laboratory data of Beeman et al (1988) for the case of lithospheric extension (ABC) and compression (*EFG*). The knee in the curves reflects an observed change in the coefficient of friction from 0.55 at low values of fault-normal stress to 0.20 at higher values of fault-normal stress. The frictional strength has negligible strain-rate sensitivity. Thus, in the case of lithospheric extension at, say, an imposed rate of 10^{-16} s^{-1}, strength at the surface (point *A*) is very low where the brittle field dominates and pressure is low. Pressure increases with depth, so strength increases along *AB*. However, temperature also increases, and at some point (*B*), the lithosphere will deform in ductile fashion as readily as it will in brittle fashion. Thereafter, ductile strength decreases and governs strength, which follows the curve *BD*. (From Beeman et al 1988.)

usually called steady-state creep), is well documented in ice at warm conditions, typically >250 K [for a thorough review, see Budd & Jacka (1989)]. For example, within about $\varepsilon = 0.10$ in pure shear, the locus of *c* axes in polycrystalline ice forms a small circle girdle around the compression direction (Jacka & Maccagnan 1984), whereas in simple shear a bimodal pattern will develop and eventually (with sufficient strain) grade to a single pole, with the basal planes aligned in the plane of shear (Bouchez & Duval 1982, Kamb 1972). The tertiary creep rate in pure shear is about three times faster than the creep rate for isotropic ice under the same stress and temperature, and about nine times faster in simple shear (Budd & Jacka 1989).

Although very much applicable to planetary science, for instance to the large strains in a pure-ice Ganymede mantle, there has been only minor evidence cited of tertiary creep in laboratory tests at planetary temperatures. The matter is by no means closed, however, because studies have not been exhaustive. For example, there has been no investigation of ice deformed in simple shear, or to very large strains (>1) at planetary conditions. The creep rate of ice I deformed in pure shear in the dislocation creep regime at $160 < T < 258$ K and $\sigma > 5$–10 MPa does not change significantly (after an early transient stage), to at least $\varepsilon = 0.30$ (Durham et al 1997). Active recrystallization driven by high dislocation densities at these stress levels may erase developing anisotropies. Durham et al (2001) see signs of extended transient strain softening at lower stresses, perhaps due to the lower driving force for recrystallization. However, recrystallization is also very active in warm samples that exhibit tertiary creep (Meglis et al 1999), and the onset of recrystallization with increased strain rate at warmer temperatures in polar ice caps produces dramatic fabric changes from anisotropic to nearly isotropic (Figure 7). Recrystallization under deviatoric stress adds another layer of complexity (Kamb 1961, Paterson 1973). Similarly to ice I at planetary temperatures, none of the higher-pressure phases, ice II, III, V, or VI, exhibits signs of tertiary creep (Durham et al 1997). There has been one direct measurement of fabric in high-pressure ice, that of Bennett et al (1997), who found that (rhombohedral) ice II deformed in axial compression developed a girdle signifying slip on prism planes (normal to the basal plane) that was measurable at $\varepsilon = 0.07$ and very strong at $\varepsilon = 0.57$.

PLANETARY APPLICATIONS

It is not the purpose of this review to critically compare planetological models that involve the rheology of water ice. This is not to say that the topic should be avoided entirely. We give a number of examples here of how ice rheology has been applied to the planets.

Thermal Evolution

Primary among the structural influences that ice exerts on icy satellites is the effect of its rheology on thermal evolution (Schubert et al 1986). Early thermal models showed that objects of mean density around 2 Mg/m^3 (i.e. roughly equal masses of silicates and ice, typical of icy moons), with diameters greater than a few hundred kilometers and chrondritic abundances of radiogenic elements in the rocky phases, would easily achieve melting in the absence of solid-state convection (Consolmagno & Lewis 1976, Lewis 1971). Once melt appears, the chance for runaway melting increases, as rocky material falling through the liquid releases its gravitational potential energy. Nonconvective models universally predict that the large low-density moons (Ganymede, Callisto, and Titan) will differentiate to a rocky core, possibly a rock plus ice lower mantle, a liquid mantle, and an ice plus rock crust.

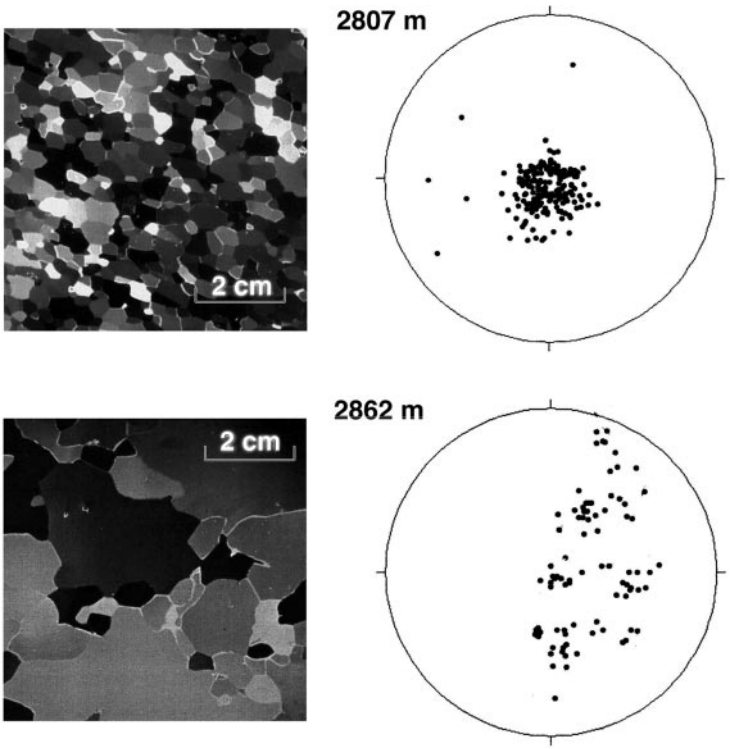

Figure 7 Illustration of the effect of dynamic recrystallization on fabric. Photographs at the left are thin sections of ice from the Greenland Ice Core Project core from depths of 2807 m and 2862 m. Stereographic projections at the right show the corresponding orientations of c axes of all the grains in the thin sections. At 2807 m, the ice has a strong *c*-axis fabric, but 55 m lower in the core, grains have recrystallized, and most of the preferred orientation has been erased. (From Thorsteinsson et al 1997.)

Convection in a layer heated from below occurs as buoyancy forces caused by thermal expansion overcome mechanical stability. The ratio of buoyancy to stability is usually stated as a dimensionless parameter called the Rayleigh number (Ra):

$$\mathrm{Ra} = (g\alpha\rho D^3 \Delta T)/\kappa\eta_{\mathrm{eff}}, \tag{27}$$

where g is the gravitational acceleration, α the coefficient of volumetric thermal expansion, ρ the density, D the layer thickness, ΔT the temperature drop across D, and κ the thermal diffusivity. As Ra increases, the likelihood of convection increases. The criterion for onset of convection is

$$\mathrm{Ra} > \mathrm{Ra}_{\mathrm{crit}}, \tag{28}$$

where Ra is of order of 10^3. Lower effective viscosity η_{eff} means less mechanical stability and increased probability of convection. Calculations using reasonable values for the viscosity of ice show that with convection, the interiors of even the largest icy satellites should not melt (Schubert et al 1986).

However, the advective transport of heat that accompanies convection is an efficient planetary cooling mechanism (thermal models usually assign an adiabatic temperature gradient to the convecting layer). Convection thus cools and lowers the buoyancy factor in Ra, making convection less likely. There is thus the possibility of planetary self-regulation, with temperatures reaching the level required to achieve the viscosity necessary to balance internal heat production. This principle was first discussed by Tozer (see Schubert et al 1981). The balance that is struck depends on the temperature dependence of η_{eff}. Thus, the rheology of ice must profoundly affect the internal structure of icy satellites and, to the extent that inner processes are expressed in crustal tectonics, the outward appearance as well. The three icy Galilean satellites, Europa, Ganymede, and Callisto, which as a result of the Galileo mission are the most heavily studied of the large icy moons, present a useful study in contrasts (Showman & Malhotra 1999). One of the outstanding questions in planetary science is the so-called Ganymede-Callisto dichotomy, the conundrum of two moons that have similar size and composition but entirely different inner structures (judged by moment of inertia) and outward appearance (McKinnon & Parmentier 1986). One must look first to the rheology of ice for an explanation.

Crater Relaxation

Satellite geotherms are typically characterized by a very cold surface (within a few 10 K of 100 K) and a steeply rising temperature-vs-depth profile. Structurally, the satellites thus resemble soft, deformable material overlain by a hard lid. Long-wavelength features such as large craters are therefore influenced by the less-viscous material at depth and thus, for instance, will develop bowed floors, whereas shorter-wavelength features such as crater rims and the entirety of smaller craters sense mostly the stiffer near-surface material (Scott 1967). Large craters invariably show a much more degraded topography with respect to smaller craters, and systematics of size vs relaxation are a quantitative probe of interior rheology (Parmentier & Head 1981).

Computer modeling suggests that despite the poor ductility of the cold surface, brittle and transitional ductile-to-brittle flow are not important processes in crater relaxation (Dombard & McKinnon 2000), except in the case of very large craters that involve long-range tectonism and crustal thinning (Allemand & Thomas 1991, Melosh 1982). Modeling is difficult, however, because few applications of laboratory data undergo the extreme strain-rate extrapolation required of crater relaxation. Predicted relaxation rates based on lab data have varied enormously. Even in models that incorporate fully non-Newtonian rheology, predictions are badly inconsistent: Thomas & Schubert (1988) assumed a pure-ice Ganymede crust and

an early version of the dislocation creep regime C (with $n = 4.7$) and found that large craters relaxed far too quickly (*e*-folding times of crater depth $\sim 10^7$ years) to be consistent with the current crater morphology on Ganymede. Dombard & McKinnon (2000) repeated that exercise, including even the softer-rheology GSS creep, yet found *e*-folding times nearly two orders of magnitude longer than those found by Thomas & Schubert (1988). The large discrepancy remains unexplained.

Phase Change and Mantle Convection

With internal pressures exceeding 2 GPa, phase changes must be ubiquitous in an icy, convecting mantle in the three low-density giants Ganymede, Callisto, and Titan (Figure 3). Because of density and entropy changes across phase boundaries, thermally driven convection of material across a phase boundary will either inhibit or assist convection, depending on the Clapeyron slope, dP/dT, of the phase boundary (Bercovici & Schubert 1986, Christensen 1995, McKinnon 1998, Schubert & Turcotte 1971). For ice I $\rightarrow$ II, the Clapeyron slope is positive (Figure 3), so a descending (and therefore cooler than its surroundings) plume of ice I will encounter the II phase boundary at lower P than if it were not convecting. The phase change therefore occurs at shallower depth than in the nonconvecting surroundings, and the increase in density of the now-transformed ice II (about 20% over ice I) drives the convection faster. Likewise, an ascending plume of ice II is warmer than its surroundings. It will encounter the ice I phase boundary at higher pressure and will therefore also drive convection. The situation reverses for a negative Clapeyron slope, as for instance with ice I $\rightarrow$ III and II $\rightarrow$ V. In that case, the descending plume becomes more buoyant than otherwise (and the descending plume less buoyant), and convection is impeded. The effect of Clapeyron slope is sufficiently strong in ice that convection may not be able to penetrate either the I–III or II–V phase boundaries (Bercovici & Schubert 1986, McKinnon 1998). By extension, there is a decreased propensity for double-layer convection through the ice I and II depths. Double-layer convection leads to significantly warmer interior temperatures, because of the presence of a nonconvecting thermal boundary layer between convecting layers. Thus, the effect of Clapeyron slope on overall thermal evolution can be profound.

There are also a number of kinetic effects related to phase changes in ice, the most pronounced of which may be the metastability of ice III in the warmer part of the phase field of ice II (Bridgman 1912, Durham et al 1988). It seems unlikely that such metastability could persist on a planetary timescale, but given (*a*) the profound nature of this metastability as viewed on the laboratory timescale, even able to withstand large ductile strains and repeated transformation back and forth to ice V, (*b*) the large viscosity contrast between ice II and III (Figure 4), and (*c*) the proximity of plausible satellite geotherms to the ice II–III phase boundary (e.g. Mueller & McKinnon 1988), the metastability should not be completely ignored by planetologists.

In the zone of transformation, kinetically limited or otherwise, there is also a brief transformation-induced weakening that can occur if the two phases physically mix during transformation and if there is a density difference between the phases. The density contrast causes local internal stresses, which are biased by the external deviatoric stress field toward producing enhanced strain rates in the direction of the applied differential stress (Poirier 1985). This transformation plasticity (sometimes called transformation superplasticity) has been observed in ice I–II and I–III cycling in the laboratory (Dunand et al 2001).

How Thin is Europa's Ice Shell?: A Case Study

Although the existence of a Europan internal ocean is not proven, current thinking centers on a differentiated Europa whose 150-km outer layer of water (Anderson et al 1998) consists of a solid ice shell overlying a liquid ocean. Tidal strains forced by an orbital resonance with Io and Ganymede (along with some amount of radiogenic heating) supply sufficient heat to keep the base of the ice shell from growing downward (Ojakangas & Stevenson 1989), and surface morphology shows plentiful signs of viscous activity not far below the rigid outer skin (Showman & Malhotra 1999). Although the Europan ice shell may well contain significant amounts of hydrated salt phases (Kargel 1998b), for which there are no rheological data, the relatively tight geological constraint on flow within the shell along with improved understanding of ice rheology from the laboratory have catalyzed modeling activity based on pure ice rheology (McKinnon 1999, Pappalardo et al 1998b).

Ojakangas & Stevenson (1989) modeled a nonconvective Europan ice shell and found that an ice thickness of roughly 25 km would dissipate the heat generated by tidal flexing through conduction alone. They may not have considered the possibility of convective overturn at this thickness because the flow law they used for ice was the terrestrially inspired Glen law for ice, $n = 3$ in Equation 10, with a very high activation energy of $Q = 139$ kJ/mol. This makes ice unrealistically hard at temperatures below about 260 K (Table 1), i.e. throughout most of the ice shell. It is interesting to note, however, that the same law applied (more appropriately) to the very warm base of the putative ice shell shows that lateral flow of soft ice will smooth any irregularities at the base, giving the shell a nearly constant thickness everywhere (Stevenson 2000).

Pappalardo et al (1998b) and McKinnon (1999) considered convective instability in a soft layer beneath a stagnant lid and used the most current laboratory-determined rheological laws for the creep of ice I, including that for GSS creep. The key parameter in convective instability criterion (Equation 28) is effective viscosity η_{eff}, which depends not only on grain size but, for a non-Newtonian material, on σ (or, equivalently, $\dot{\varepsilon}$) as well (Equation 19). The Pappalardo et al (1998b) approach is to assume that convective strain rate is roughly the same as the relatively fast cyclic tidal strain rate of approximately 2×10^{-10} s^{-1} (Ojakangas & Stevenson 1989) and to assume that grain size ranges from 0.1 mm in the

cool portions to 10 mm in warmer portions of the ice shell. Given a reasonable temperature gradient, η_{eff} is then calculated from Equations 10 and 19. Pappalardo et al (1998b) find that the applicable creep regime is GSS, and that convective instability must develop for a ductile sublayer thickness of 2–8 km and a total shell thickness of 6–26 km (as recalculated by McKinnon 1999). The spacing of Europa's ubiquitous domes and pits is in fact roughly twice the thickness of the sublayer, consistent with their apparent diapiric origin (Pappalardo et al 1998b).

McKinnon (1999) made several refinements to the Pappalardo et al (1998b) calculations but ended up with roughly the same ice shell thickness. Making simplifying assumptions about some of the parameters in Equation 27, he compared the curve of effective viscosity vs convecting layer thickness at the onset of convection, $\text{Ra} = \text{Ra}_{\text{crit}}$, to effective viscosities calculated from the creep law for ice (Equation 10, Table 1). His key assumption was that the viscosity from Equation 10 was, with a geometric correction, the same viscosity that corresponded to the tidal strain rate of $2 \times 10^{-10}\ \text{s}^{-1}$. He also showed that the (essentially constant) temperature in the actively convecting layer is approximately 260 K. Thus, for ice deforming by dislocation creep, McKinnon found that the Europan ice shell had to be >50 km thick. However, for grain size $d < 1$ mm, GSS creep produces a lower viscosity than dislocation creep, so shell thickness then becomes a function of d. Using the d-vs-σ relationship (Equation 25) with $m = 1$ as a further constraint, McKinnon concluded that grain sizes in the convecting Europan shell were <1 mm and a total shell thickness of approximately 30 km could be expected.

It is remarkable that even with the bare minimum of experimental and observational constraint, these models predict the thin, soft ice shell with overlying hard crust that such surface activities as crater relaxation (Thomas & Schubert 1986) and cycloidal fractures (Hoppa et al 1999) seem to require. The intriguing possibility of a current-day internal ocean on Europa will surely encourage further work. The next stage may involve modeling grain growth in the Europan ice shell. As discussed above, unless limited by second-phase pinning of grain boundaries or by a steady supply of intracrystalline defects, grain size will theoretically grow without limit. GSS creep alone creates no crystal defects, so the dynamic picture in the models of Pappalardo et al (1998b) and McKinnon (1999) is incomplete. Of course, laws for grain growth in ice at temperatures lower than terrestrial still suffer from lack of laboratory constraint.

CONCLUSION

Flow parameters have been measured for what are plausibly the mechanisms responsible for solid-state deformation on and within the icy moons, but a more fundamental understanding of the underlying deformation physics is needed before we can extrapolate reliably to conditions outside those accessible in the laboratory.

Recent discoveries of grain-boundary-related mechanisms and evidence that grain size may self regulate at mechanism boundaries on the deformation map are intriguing first steps in this direction, but for now the large strain rate extrapolations in Figures 2, 4, 5, and 6 must be considered mostly empirical. Other important deficiencies exist in our understanding of the roles of impurities and second phases. The former has seen almost no research at conditions beyond terrestrial, for instance, and only limited experimental work has been directed toward the rheology of mixed-phase icy solids, a topic that has been purposely excluded from this review.

Is the task hopeless? Certainly not. The questions we identify today, such as the effect of hydrated salts on the rheology of Europa's ice shell, or which mechanism of deformation governs (or governed) the internal dynamics on a Ganymede, are considerably more sophisticated than those posed a quarter century ago, when the first evolutionary models appeared. We can assume that further space-based observations will drive better models of crustal deformation and evolution, which will in turn influence the direction of laboratory investigations.

ACKNOWLEDGMENTS

We thank several people for sharing their thoughts and prepublication manuscripts with us, including H de Bresser, A Dombard, D Dunand, D Goldsby, M Mellon, and J Nye. We thank S Durham and M Mellon for their critical comments. We are especially grateful to D Goldsby and D Kohlstedt for their patience during extended discussions about competing flow mechanisms in ice, as well as for providing Figure 2. This work was supported by NASA under order W-19,075. Work was also performed under the auspices of the US Department of Energy by the Lawrence Livermore National Laboratory under contract W-7405-ENG-48.

LITERATURE CITED

Allemand P, Thomas PG. 1991. The thermal gradient of Callisto constrained by Asgard basin: rheological and chemical implications. *J. Geophys. Res.* 96:20981–88

Alley RB. 1992. Flow-law hypotheses for ice-sheet modeling. *J. Glaciol.* 38:245–56

Alley RB, Perepezko JH, Bentley CR. 1986. Grain growth in polar ice. II. Application. *J. Glaciol.* 32:425–33

Alley RB, Woods GA. 1996. Impurity influence on normal grain growth in the GISP2 ice core, Greenland. *J. Glaciol.* 42:255–60

Anderson JD, Lau EL, Sjogren WL, Schubert G, Moore WB. 1998. Europa's differentiated internal structure: inferences from two Galileo encounters. *Science* 276:1236–39

Arena L, Nasello OB, Levi L. 1997. Effect of bubbles on grain growth in ice. *J. Phys. Chem. B* 101:6109–12

Azuma N. 1994. A flow law for anisotropic ice and its application to ice sheets. *Earth Planet. Sci. Lett.* 128:601–14

Baker RW, Gerberich WW. 1979. The effect of crystal size and dispersed-solid inclusions

on the activation energy for creep of ice. *J. Glaciol.* 24:179–94

Beeman M, Durham WB, Kirby SH. 1988. Friction of ice. *J. Geophys. Res.* 93:7625–33

Bennett K, Wenk H-R, Durham WB, Stern LA, Kirby SH. 1997. Preferred crystallographic orientation in the ice I → II transformation and the flow of ice II. *Philos. Mag. A* 76:413–35

Bercovici D, Schubert G. 1986. Phase transitions and convection in icy satellites. *Geophys. Res. Lett.* 13:448–51

Bouchez JL, Duval P. 1982. The fabric of polycrystalline ice deformed in simple shear: experiments in torsion, natural deformation and geometrical interpretation. *Textures Microstruct.* 5:171–90

Bridgman PW. 1912. Water, in the liquid and five solid forms, under pressure. *Proc. Am. Acad. Arts Sci.* 47:347–438

Brown ME, Calvin WM. 2000. Evidence for crystalline water and ammonia ices on Pluto's satellite Charon. *Science* 287:107–9

Budd WF, Jacka TH. 1989. A review of ice rheology of ice sheet modelling. *Cold Reg. Sci. Technol.* 16:107–44

Burns J, Matthews MS, eds. 1986. *Satellites.* Tucson: Univ. Ariz. Press

Christensen U. 1995. Effects of phase transitions on mantle convection. *Annu. Rev. Earth Planet. Sci.* 23:65–87

Clark B, Mullin R. 1976. Martian glaciation and the flow of solid CO_2. *Icarus* 27:215–28

Clark RN, Fanale FP, Gaffey MJ. 1986. Surface composition of natural satellites. See Burns & Matthews 1986, pp. 437–91

Consolmagno GJ, Lewis JS. 1976. Structural and thermal models of icy Galilean satellites. In *Jupiter*, ed. T Gehrels, pp. 1035–51. Tucson: Univ. Ariz. Press

Cruikshank DP, Brown RH, Calvin WM, Roush TL, Bartholomew MJ. 1998a. Ices on the satellites of Jupiter, Saturn, and Uranus. See Schmitt et al 1998, pp. 579–606

Cruikshank DP, Roush TL, Owen TC, Geballe TR, de Bergh C, et al. 1993. Ices on the surface of Triton. *Science* 261:742–45

Cruikshank DP, Roush TL, Owen TC, Quirico E, de Bergh C. 1998b. The surface compositions of Triton, Pluto and Charon. See Schmitt et al 1998, pp. 655–84

Dash JG, Hu H, Wettlaufer JS. 1995. The premelting of ice and its environmental consequences. *Rep. Prog. Phys.* 58:115–67

de Bresser JHP, Peach CJ, Reijs JPJ, Spiers CJ. 1998. On dynamic recrystallization during solid-state flow: effects of stress and temperature. *Geophys. Res. Lett.* 25:3457–60

de Bresser JHP, ter Heege JH, Spiers CJ. 2001. Grain size reduction by dynamic recrystallization: Can it result in major rheological weakening? *J. Earth Sci.* In press. http://dx.doi.org/10.1007/s005310000149

de la Chapelle S, Castelnau O, Lipenkov V, Duval P. 1998. Dynamic recrystallization and texture development in ice as revealed by the study of deep ice cores in Antarctica and Greenland. *J. Geophys. Res.* 103:5091–105

Derby B. 1990. Dynamic recrystallization and grain size. In *Deformation Processes in Minerals, Ceramics and Rocks*, ed. DJ Barber, PG Meredith, pp. 354–64. London: Unwin Hyman

Derby B, Ashby MF. 1987. On dynamic recrystallisation. *Scr. Metall.* 21:879–84

Dimitrov VI, Bar-Nun A. 1999. Admissible height of local roughness of Titan's landscape. *J. Geophys. Res.* 104:5933–38

Dombard AJ, McKinnon WB. 2000. Long-term retention of impact crater topography on Ganymede. *Geophys. Res. Lett.* 27:3663–66

Dunand DC, Schuh C, Goldsby DL. 2001. Pressure-induced transformation plasticity of H_2O ice. *Phys. Rev. Lett.* 86:668–71

Durham WB, Heard HC, Kirby SH. 1983. Experimental deformation of polycrystalline H_2O ice at high pressure and low temperature: preliminary results. *J. Geophys. Res.* 88:B377–92

Durham WB, Kirby SH, Heard HC, Stern LA, Boro CO. 1988. Water ice phases II, III, and V: plastic deformation and phase relationships. *J. Geophys. Res.* 93:10191–208

Durham WB, Kirby SH, Stern LA. 1992. Effects of dispersed particulates on the rheology of water ice at planetary conditions. *J. Geophys. Res.* 97:20883–97

Durham WB, Kirby SH, Stern LA. 1993. Flow of ices in the ammonia-water system. *J. Geophys. Res.* 98:17667–82

Durham WB, Kirby SH, Stern LA. 1997. Creep of water ices at planetary conditions: a compilation. *J. Geophys. Res.* 102:16293–302

Durham WB, Stern LA, Kirby SH. 1996. Rheology of water ices V and VI. *J. Geophys. Res.* 101:2989–3001

Durham WB, Stern LA, Kirby SH. 1999. Steady-state flow of solid CO_2. *Geophys. Res. Lett.* 26:3493–96

Durham WB, Stern LA, Kirby SH. 2001. The rheology of ice I at low stress and elevated confining pressure. *J. Geophys. Res.* In press

Duval P, Lliboutry L. 1985. Superplasticity owing to grain growth in polar ices. *J. Glaciol.* 31:60–62

Echelmeyer K, Kamb B. 1986. Rheology of ice II and ice III from high-pressure extrusion. *Geophys. Res. Lett.* 13:693–96

Ellsworth K, Schubert G. 1983. Saturn's icy satellites: thermal and structural models. *Icarus* 54:490–510

Eluszkiewicz J, Stevenson DJ. 1990. Rheology of solid methane and nitrogen: applications to Triton. *Geophys. Res. Lett.* 17:1753–56

Engelder T. 1994. Deviatoric stressitis: a virus infecting the earth science community. *Eos Trans. AGU* 75:209–10

Evans B, Kohlstedt DL. 1995. Rheology of rocks. In *Rock Physics and Phase Relations: A Handbook of Physical Constants*, ed. TJ Ahrens, 3:148–65. Washington, DC: Am. Geophys. Union

Fink J, Gault D, Greeley R. 1984. The effect of viscosity on impact cratering and possible application to the icy satellites of Saturn and Jupiter. *J. Geophys. Res.* 89:417–23

Fletcher NH. 1970. *The Chemical Physics of Ice* . New York: Cambridge Univ. Press. 271 pp.

Frost HJ, Ashby MF. 1982. *Deformation Mechanism Maps*. New York: Pergamon. 167 pp.

Glen JW. 1952. Experiments on the deformation of ice. *J. Glaciol.* 2:111–14

Glen JW. 1955. The creep of polycrystalline ice. *Proc. R. Soc. London Ser. A* 228:519–38

Goldsby DL, Kohlstedt DL. 1997. Grain boundary sliding in fine-grained ice I. *Scr. Mater.* 37:1399–406

Goldsby DL, Kohlstedt DL. 2001. Superplastic deformation of ice. I. Experimental observations. *J. Geophys. Res.* In press

Golombek MP, Banerdt WB. 1986. Early thermal profiles and lithospheric strength of Ganymede from extensional and tectonic features. *Icarus* 68:252–65

Goodman DJ, Frost HJ, Ashby MF. 1981. The plasticity of polycrystalline ice. *Philos. Mag.* 43:665–95

Gow AJ. 1969. On the rates of growth of grains and crystals in south polar firn. *J. Glaciol.* 8:241–52

Herrick DL, Stevenson DJ. 1990. Extensional and compressional instabilities in icy satellite lithospheres. *Icarus* 85:191–204

Hill R. 1950. *The Mathematical Theory of Plasticity*. Oxford, UK: Oxford Univ. Press. 355 pp.

Hooke RL, Dahlin BB, Kauper MT. 1972. Creep of ice containing dispersed fine sand. *J. Glaciol.* 11:327–36

Hoppa GV, Tufts RB, Greenberg R, Geissler PE. 1999. Formation of cycloidal features on Europa. *Science* 285:1899–902

Jacka TH, Li J. 1994. The steady state crystal size of deforming ice. *Ann. Glaciol.* 20:13–18

Jacka TH, Maccagnan M. 1984. Ice crystallographic and strain rate changes with strain in compression and extension. *Cold Reg. Sci. Technol.* 8:269–86

Jaeger JC. 1969. *Elasticity, Fracture and Flow*. London: Methuen. 268 pp. 3rd. ed.

Jaeger JC, Cook NGW. 1976. *Fundamentals of Rock Mechanics*. London: Chapman & Hall. 585 pp. 2nd ed.

Johnson TV, McGetchin TR. 1973. Topography on satellite surfaces and the shape of asteroids. *Icarus* 18:612–20

Kamb B. 1964. Glacier geophysics. *Science* 146:353–65

Kamb B. 1972. Experimental recrystallization of ice under stress. In *Flow and Fracture of Rocks*, ed. HC Heard, IY Borg, NL Carter, CB Raleigh, pp. 211–41. Washington, DC: Am. Geophys. Union

Kamb WB. 1961. The thermodynamic theory of nonhydrostatically stressed solids. *J. Geophys. Res.* 66:259–71

Kargel J. 1998a. Physical chemistry of ices in the outer solar system. See Schmitt et al 1998, pp. 3–32

Kargel JS. 1998b. The salt of Europa. *Science* 280:1211–12

Kirby SH, Durham WB, Beeman ML, Heard HC, Daley MA. 1987. Inelastic properties of ice Ih at low temperatures and high pressures. *J. Phys.* 48 (Suppl.):227–32

Kirby SH, Durham WB, Stern LA. 1992. The ice I → II transformation: mechanisms and kinetics under hydrostatic and nonhydrostatic conditions. In *Physics and Chemistry of Ice*, ed. N Maeno, T Hondoh, pp. 456–63. Sapporo, Jpn.: Hokkaido Univ. Press

Kirk RL, Stevenson DJ. 1987. Thermal evolution of a differentiated Ganymede and implications for surface features. *Icarus* 69:91–134

Kivelson MG, Khurana KK, Russell CT, Volwerk M, Walker RJ, Zimmer C. 2000. Galileo magnetometer measurements: a stronger case for a subsurface ocean at Europa. *Science* 289:1340–43

Langdon TG. 1996. Transitions in creep behavior. *Mater. Transact., Jpn. Inst. Metals* 37:359–62

Langdon TG, Mohamed FA. 1977. The characteristics of independent and sequential creep processes. *J. Aust. Inst. Metall.* 22:189–99

Lange MA, Ahrens TJ. 1987. Impact experiments in low-temperature ice. *Icarus* 69:506–18

Lewis JS. 1971. Satellites of the outer plants: their physical and chemical nature. *Icarus* 15:174–85

Lewis JS. 1972. Low temperature condensation from the solar nebula. *Icarus* 16:241–52

Macosko CW. 1994. *Rheology: Principles, Measurements, and Applications*. New York: VCH. 550 pp.

Marcialis RL, Rieke GH, Lebofsky LA. 1987. The surface composition of Charon: tentative identification of water ice. *Science* 237:1349–51

McKinnon WB. 1998. Geodynamics of icy satellites. See Schmitt et al 1998, pp. 525–50

McKinnon WB. 1999. Convective instability in Europa's floating ice shell. *Geophys. Res. Lett.* 26:951–54

McKinnon WB, Parmentier EM. 1986. Ganymede and Callisto. See Burns & Matthews 1986, pp. 718–63

Meglis IL, Melanson PM, Jordaan IJ. 1999. Microstructural change in ice. II. Creep behavior under triaxial stress conditions. *J. Glaciol.* 45:438–48

Melosh HJ. 1982. A simple mechanical model of Valhalla basin, Callisto. *J. Geophys. Res.* 87:1880–90

Mendelson A. 1968. *Plasticity: Theory and Application*. New York: Macmillan. 353 pp.

Mueller S, McKinnon WB. 1988. Three-layered models of Ganymede and Callisto: compositions, structures, and aspects of evolution. *Icarus* 76:437–64

Nayar HS, Lenel FV, Ansell GS. 1971. Creep of dispersions of ultrafine amorphous silica in ice. *J. Appl. Phys.* 42:3786–89

Nye JF. 1957. The distribution of stress and velocity in glaciers and ice-sheets. *Proc. R. Soc. London Ser. A* 239:113–33

Nye JF. 2000. A flow model for the polar ice caps of Mars. *J. Glaciol.* 46:438–44

Ojakangas GW, Stevenson DJ. 1989. Thermal state of an ice shell on Europa. *Icarus* 81:220–41

Pappalardo RT, Head JW, Collins GC, Kirk RL, Neukum G, et al. 1998a. Grooved terrain on Ganymede: first results from Galileo high-resolution imaging. *Icarus* 135:276–302

Pappalardo RT, Head JW, Greeley R, Sullivan RJ, Pilcher C, et al. 1998b. Geological

evidence for solid-state convection in Europa's ice shell. *Nature* 391:365–68
Parmentier EM, Head JW. 1981. Viscous relaxation of impact craters on icy planetary surfaces: determination of viscosity variation with depth. *Icarus* 47:100–11
Parmentier EM, Squyres SW, Head JW, Allison ML. 1982. The tectonics of Ganymede. *Nature* 295:290–93
Paterson MS. 1973. Nonhydrostatic thermodynamics and its geologic applications. *Rev. Geophys. Space Phys.* 11:355–89
Paterson MS. 1978. *Experimental Rock Deformation—The Brittle Field*. Berlin: Springer. 254 pp.
Paterson MS. 1987. Problems in the extrapolation of laboratory rheological data. *Tectonophysics* 133:33–43
Paterson WSB. 1994. *The Physics of Glaciers*. Oxford: Pergammon. 250 pp.
Peltier WR, Goldsby DL, Kohlstedt DL, Tarasov L. 2000. Ice age ice sheet rheology: constraints from the Last Glacial Maximum form of the Laurentide ice sheet. *Ann. Glaciol.* 30:163–76
Petrenko VF, Whitworth RW. 1999. *Physics of Ice*. New York: Oxford. 373 pp.
Poirier J-P. 1985. *Creep of Crystals*. New York: Cambridge Univ. Press. 260 pp.
Poirier J-P, Sotin C, Peyronneau J. 1981. Viscosity of high-pressure ice VI and evolution and dynamics of Ganymede. *Nature* 292:225–27
Porter DA, Easterling KE. 1992. *Phase Transformations in Metals and Alloys*. New York: Chapman & Hall. 514 pp.
Prinn RG, Fegley B Jr. 1981. Kinetic inhibition of CO and N_2 reduction in circumplanetary nebulae: implications for satellite composition. *Astrophys. J.* 249:308–17
Raj R, Ghosh AK. 1981. Micromechanical modelling of creep using distributed parameters. *Acta Metall.* 29:283–92
Reynolds RT, Cassen PM. 1979. On the internal structure of the major satellites of the outer planets. *Geophys. Res. Lett.* 6:121–24
Rist MA, Murrell SAF. 1994. Ice triaxial deformation and fracture. *J. Glaciol.* 40:305–18
Schenk PM. 1993. Central pit and dome craters: exposing the interiors of Ganymede and Callisto. *J. Geophys. Res.* 98:7475–98
Schenk PM, Moore JM. 1998. Geologic landforms and processes on icy satellites. See Schmitt et al 1998, pp. 551–78
Schubert G, Spohn T, Reynolds RT. 1986. Thermal histories, compositions and internal structures of the moons of the solar system. See Burns & Matthews 1986, pp. 224–92
Schubert G, Stevenson DJ, Ellsworth K. 1981. Internal structures of the Galilean satellites. *Icarus* 47:46–59
Schubert G, Turcotte DL. 1971. Phase changes and mantle convection. *J. Geophys. Res.* 76:1424–32
Schmitt B, de Bergh C, Festou M, eds. 1998. *Solar System Ices*. Dordrecht, Netherlands: Kluwer
Scott RF. 1967. Viscous flow of craters. *Icarus* 7:139–48
Shimizu I. 1998. Stress and temperature dependence of recrystallized grain size: a subgrain misorientation model. *Geophys. Res. Lett.* 25:4237–40
Showman AP, Malhotra R. 1999. The Galilean satellites. *Science* 286:77–84
Sotin C, Gillet P, Poirier J-P. 1985. Creep of high-pressure ice VI. In *Ices in the Solar System*, ed. J Klinger, D Benest, A Dollfus, R Smoluchowski, pp. 109–18. Dordrecht, Netherlands: Reidel
Sotin C, Poirier J-P. 1987. Viscosity of ice V. *J. Phys.* 48(Suppl.):233–38
Stern LA, Durham WB, Kirby SH. 1997. Grain-size-induced weakening of H_2O ices I and II and associated anisotropic recrystallization. *J. Geophys. Res.* 102:5313–25
Stern LA, Kirby SH, Durham WB. 1996. Peculiarities of methane clathrate hydrate formation and rheology, and the associated superheating of water ice. *Science* 273:1843–48
Stevenson DJ. 2000. Limits on the variation of thickness of Europa's ice shell. In *Lunar and Planetary Science XXXI*, Abstr. 1506. Houston, TX: Lunar Planet. Inst. (CD-ROM)

Thomas PJ, Schubert G. 1986. Crater relaxation as a probe of Europa's interior. *J. Geophys. Res.* 91:D453–59

Thomas PJ, Schubert G. 1987. Finite element models of non-Newtonian crater relaxation. *J. Geophys. Res.* 92:749–58

Thomas PJ, Schubert G. 1988. Power law rheology of ice and the relaxation style and retention of craters on Ganymede. *J. Geophys. Res.* 93:13755–62

Thorsteinsson T, Kipfstuhl J, Eicken H, Johnsen SJ, Fuhrer K. 1995. Crystal size variations in Eemian-age ice from the GRIP ice core, Central Greenland. *Earth Planet. Sci. Lett.* 131:381–94

Thorsteinsson T, Kipfstuhl J, Miller H. 1997. Texture and fabrics in GRIP core. *J. Geophys. Res.* 102:26583–99

Twiss RJ. 1977. Theory and applicability of a recrystallized grain size paleopiezometer. *Pageoph. Pure Appl. Geophys.* 115:227–44

Weertman J. 1968. Dislocation climb theory of steady state creep. *Transact. Am. Soc. Metall.* 61:681–94

Weertman J. 1973. Creep of ice. In *Physics and Chemistry of Ice*, ed. E Whalley, SJ Jones, LW Gold, pp. 320–37. Ottawa, Que.: R. Soc. Can.

Weertman J. 1983. Creep deformation of ice. *Annu. Rev. Earth Planet. Sci.* 11:215–40